Deployment of a Bubble Chamber for Dark Matter Searches

Marta Neves dos Reis[1]

[1]*Departamento de Física, Instituto Superior Técnico, Universidade de Lisboa, Lisbon, Portugal*

Dark matter is one of the top unsolved mysteries in physics. Its existence is well-established although its nature remains unknown. The goal of this work is to construct, control and instrument a bubble chamber detector precisely for dark matter searches. The developed work took place at Centro Tecnológico e Nuclear in Bobadela, Portugal, where the SIMPLE Lx laboratory is sited. SIMPLE is a direct dark matter detection experiment which uses superheated liquids to search one of the most popular candidates to explain dark matter, a weakly interacting massive particle (WIMP). My work consisted in developing a bubble chamber detector that could held up to 16 bars of pressure. An automaton system was adapted and rebuilt to operate the bubble chamber, and two routines were created to control it. The SIMPLE team uses acoustics to detect the nucleation signals produced in the bubble chamber. Two new acquisition channels were introduced, an acoustic one, using an hydrophone and a visual one, using a camera. Finally, the results were analyzed concluding that it is possible, with the used acoustic recording devices and the constructed bubble chamber, to pursue the nature of dark matter.

I. INTRODUCTION

In 2012, the SIMPLE Collaboration imposed the most stringent constraint (Spin-Dependent) on the dark matter exclusion plot, contributing to reduce the possible window of existence of a WIMP particle to explain the dark matter phenomenon. SIMPLE obtained this result while working with superheated droplet detectors (SDDs) although, to remain competitive with other experiments in the field, it needed to increase the total active mass. The encountered solution was to substitute the SDDs in the search for dark matter, with a bubble chamber, increasing the active mass in more that 2000%.

This paper describes precisely the complete deployment, i.e., construction, instrumentation, and analysis of acoustic results from particle calibrations, of a bubble chamber detector for dark matter searches.

It is organized as follows. Section II refers the evidences for dark matter existence, presents the candidates to explain its nature and mentions the experiments directly or indirectly searching for it. Section III explains the physics of a bubble chamber detector, mentioning the constraints necessary for it to be suitable for dark matter searches. Section IV presents the development of the detector, starting with the construction of its body and then the cap, followed by the automaton system to operate it along with the routines that control the automaton. The last subsections mention the recording devices used and the experimental apparatus, followed by and the two prototypes build. Section V presents the signal and results analysis where it is explained how to analyze a nucleation signal and how to extract conclusions about the characteristics of the event. Furthermore, an histogram is presented which leans to event discrimination between alpha and neutrons induced particles. Conclusions are drawn at the end.

II. DARK MATTER

According to the latest data provided by ESA's Planck satellite [1], dedicated to the study of the early Universe and its subsequent evolution, the baryonic matter constitutes only 4.9% of the total amount of matter and energy in the Universe. The largest contribution, 68.3% is assured by dark energy, which is thought to be the cause of the accelerated expansion of the universe. And the remaining percentage, 26.8%, is attributed to a type of matter that doesn't interact with light and hasn't yet been seen experimentally – dark matter (DM).

A. Evidences

The existence of this esoteric type of matter has been well-established and recognized, and the evidences for its existence come from several astronomical observations.

On a galactic scale, a direct evidence for DM's existence comes from the observation of rotation curves of galaxies, namely the graph of orbital velocities of stars and gas as a function of their distance to the galactic center. According to Newtonian dynamics, the rotational velocity of an object on a stable orbit with radius r is expected to be

$$v(r) = \sqrt{\frac{GM(r)}{r}} \tag{1}$$

where $M(r) = 4\pi \int \rho(r) r^2 dr$ is the mass inside the orbit considered, and $\rho(r)$ is the mass density profile.

However, instead of falling $\propto 1/\sqrt{r}$ beyond the optical disk, the observed rotation curves exhibit a characteristic flat behavior at large distances, far beyond the visible edge of the galaxy disks. This can be explained by the existence of a non-luminous dark matter halo with $M(r) \propto r$ and $\rho \propto 1/r^2$.

One other evidence comes from the weak gravitational lensing phenomenon observed when light coming from distant galaxies is sheared by large-scale structures. This effect allows one to create a map of the total matter in the observed region of the Universe which, when compared to the distribution of baryonic matter given by optical and X-ray data, reveals where dark matter is likely present. Evidence for dark matter was found when applying these concepts to the Bullet Cluster, where two clusters of galaxies are colliding. The observations show that most of the matter resided in a location different from the plasma of the galaxy (which underwent frictional interactions during the merger and slowed down). This gives a clear indication that a majority of the mass

is not only dark in nature, but also weakly interacting.

B. Candidates

The real challenge in dark matter physics lies in the study of its nature. So far, despite all the experiments working towards this goal, there is still not an answer to the questions of what is dark matter after all.

On an astronomical scale, the MACHO (Massive Astrophysical Compact Halo Object) is the simplest candidate. These objects are made of ordinary matter, such as neutron stars, black holes, brown dwarfs or unassociated planets that would emit very little to no radiation at all, making them hard to detect. Astronomical searches using gravitational microlensing have been performed and found some astronomical objects with these characteristics, although the analysis of a typical galactic dark matter halo, gives a MACHO fraction of only 20%, meaning that MACHOs can't constitute all the DM observed.

When considering a particle candidate to explain the nature of dark matter, one should recur to the zoo of particles contemplated in the Standard Model (SM) of particle physics. The SM is the most reliable and up to date model that is able to describe theoretically all the known particles and interactions, leading to good a agreement with experiments.

The SM neutrinos would constitute a good candidate for dark matter, since they have very small masses and don't interact electromagnetically neither through the strong force, being therefore, hard to detect. However, large scale structure constrains them to make up only a few percent of the total dark matter.

Beyond the SM, one can group the stable, neutral candidates for DM, with a mass from bellow GeV/c^2 to several TeV/c^2, under the WIMP designation – Weakly Interacting Massive Particles. They interact with ordinary matter through elastic scattering on nuclei and the expected interaction rate depends on the WIMP mass and on the cross section of the event. There are two distinct theories proposing a DM candidate, the Supersymetry (SUSY) which proposes the neutralino, and the Extra Dimensions theory which proposes as a WIMP candidate the Lightest Kaluza Particle.

C. Experiments Searching for DM

Many efforts have been made to detect an experimental signature of dark matter, some through direct detection experiments, via scattering of a DM particle on a target nuclei, others through indirect means, by searching for signals from annihilation or decay products of such a particle. So far, none of these experiments have been able to detect the desired experimental signature being only able to impose constraints in the mass spectrum.

The processes of DM particle annihilation or decay originates neutrinos, gamma rays, positrons, electrons, among other particles. The strongest limits on high-energy neutrinos coming from the Sun are placed by IceCube and Super- Kamiokande. For highly energetic gamma-rays (TeV) upper limits have been derived by the indirect detection experiments MAGIC, HESS and VERITAS telescopes.

Direct detection experiments, study the nuclear recoil produced by dark matter particle scattering. The recoil of the nucleus is converted into, for example, electrons, photons and phonons which can be detected by ionization, scintillation and thermal detectors, respectively. Among those with highest sensitivities are cryogenic experiments operated at sub-Kelvin temperatures; detectors based on liquefied argon or xenon; and superheated liquid detectors.

The low mass region of the spectrum is accessible by detectors with very low energy threshold and/or lighter target nuclei, while the higher mass region is probed by experiments with very low background rates and high target masses. For low WIMP masses (below 10 GeV), the tightest constraints are derived from CRESST, EDELWEISS and SuperCDMS. The most constraining upper limits for WIMP masses come from the LUX experiment using a liquid xenon time-projection chamber.

The current experimental upper limits for spin-dependent WIMP-proton and spin-independent WIMP-nucleon cross-sections, as a function of the WIMP mass, are summarized in Fig.1.

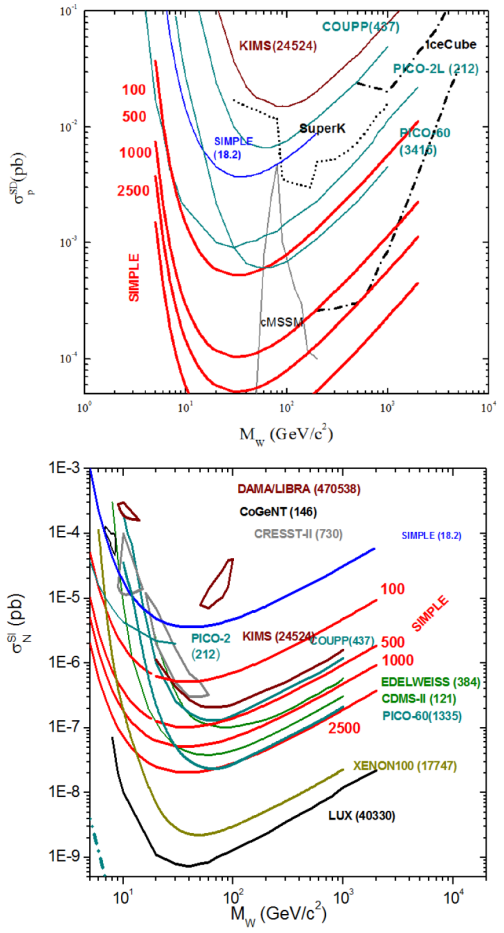

FIG. 1: Spin-dependent limits on the WIMP-proton scattering cross-section (up); Spin-independent WIMP-nucleon scattering (down), both as a function of the WIMP mass. Figure from [2].

The spin-dependent (SD) interactions result from the coupling of a WIMP's spin to the spin content of a nucleon. The cross-section for spin-dependent interactions

is proportional to J(J+1), J being the total nuclear spin, rather than to the number of nucleons, so, little is gained by using heavier target nuclei. On the contrary, for spin-independent (SI) scattering the cross-section does not depend on spin and increases dramatically with the mass of the target nuclei.

The most competitive experiments in the spin-dependent channel are PICO and SIMPLE [3]. These are both superheated liquid detector experiments. PICO uses a bubble chamber filled with C_3F_8 and SIMPLE uses superheated droplet detectors (SDDs) with freon C_2ClF_5 as their active mass.

Taking into account Fig.1, one can see the SIMPLE projection curves, represented in red, for a "zero background" 100, 500, 1000, 2500 kgd exposure measurements. These curves give sensitivities of order 10^{-4}pb for SD and 10^{-7}pb for SI. These projections represent the ambition of the new phase of SIMPLE, in which the SDDs are replaced by bubble chamber detectors. This will allow an increase in active mass and to diminish the data acquisition time.

III. PHYSICS OF A BUBBLE CHAMBER DETECTOR

A bubble chamber is based on the observation that ionizing radiations can nucleate bubbles in superheated liquids (SHL).

Considering the phase diagram of Fig.2, one knows that, whenever through the action of pressure or temperature, the substance crosses the lines that separates one state from the other, it suffers a phase transition. The metastable state is obtained precisely when this passage happens without a phase transition associated with it.

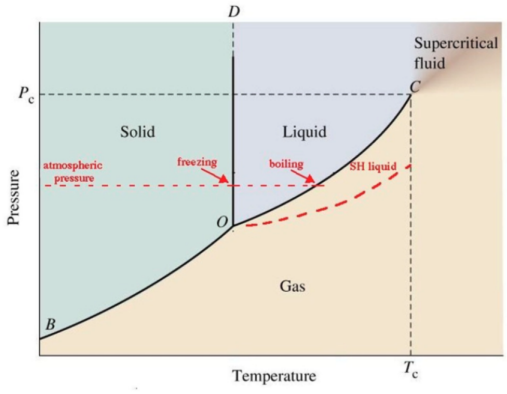

FIG. 2: Phase diagram. By decreasing the pressure or increasing the temperature, a superheated liquid can be formed within the region defined by the red dashed curve (fig. from [6]).

The state of superheat is achieved when, by changing the temperature at constant pressure, to a value above its boiling point or by isothermal expansion, to a value of pressure below its vapor pressure, the substance remains a liquid (instead of becoming a gas as its thermodynamical parameters suggest).

Once in this metastable state, the liquid can undergo violent phase transitions - nucleations - with the slightest perturbation (energy deposition). These nucleations can be of two different types depending on their origin.

- Homogeneous nucleation – occurs when a SHL is unstable as a result of local thermal agitation and spontaneously vaporizes without irradiation. This can be due to impurities containing pockets of gas in the liquid or even due to the liquid-container interface.
- Heterogeneous nucleation – consist of density fluctuations at the molecular level (as in irradiations) that are sufficient to create spontaneously expanding bubbles.

The original theory for how bubbles are created in a superheated liquid was proposed by Seitz in 1958 [5] and is often referred to as the Seitz hot spike model.

The formation process of a macroscopic bubble can be split into two parts: firstly there is the formation of a microscopic protobubble, and secondly it may or may not grow into a macroscopic, gas-filled, bubble. The conditions that determine whether or not this second step happens are the critical energy deposited by the incident radiation and the length upon which the incident particle/radiation deposits its energy.

In order to have expasion of a protobubble it is require that it achieves a critical radius defined as,

$$r_c = \frac{2\sigma}{\Delta p} \tag{2}$$

Where $\Delta p = p_b - p_l$ with p_b the vapor pressure inside the bubble and p_l the outer liquid pressure. The bubbles that happen to be generated with a radius smaller than the critical radius will be squeezed by the pressure of the liquid and collapse. Otherwise they will allow themselves to grow using as fuel the surrounding liquid.

The difference in pressure between the vapor pressure (p_b) and the operating pressure of a bubble chamber is known as "degree of superheat". The higher this degree is, the less stable the liquid is, and the bubble chamber becomes more sensitive to lower energy particles that can interact with the nuclei of the liquid creating lower energy recoils.

Critical Energy

The energy necessary to form a bubble of critical size is,

$$E_c = W_s + W_b = 4\pi r_c^2 \left(\sigma - T\frac{\partial\sigma}{\partial T}\right) + \frac{4\pi}{3} r_c^3 \rho_b (h_b - h_l) \tag{3}$$

where the first term is the work required for the surface formation of the bubble and the second term, the work required for the vaporization of the liquid inside it.

The thermodynamical irreversible work components account for the kinetic energy imparted by the expanding bubble against its wall, the energy lost through viscosity, the acoustic energy propagated as sound waves, and the thermal energy lost during expansion. These irreversible components contribute $< 1\%$ and are usually neglected.

LET Critical

Assuming that the deposited energy was sufficient, i.e., $\geq E_c$, the Linear Energy Transfer (LET) imposes that it has to be deposited in a critical range, proportional to r_c, so as to ensure its local availability for protobubble formation. It can be expressed according to,

$$\frac{dE}{dx} > \frac{E_c}{\Lambda r_c} \tag{4}$$

where dE/dx is the stopping power and Λ is a unitless scaling parameter which can be interpreted as in how many critical radius measurements do we want the energy to be concentrated in. SIMPLE uses $\Lambda = 1.40 \pm 0.05$.

A deposited energy greater than E_c, within a given length Λr_c, will trigger a phase transition.

A. DM Constraints

To be used as dark matter detectors, bubble chambers need to be able to reach a quasi continuously sensitive operation, in order to detect the desired rare event. Whenever a dark matter particle crosses the detector and interacts with it, the system has to recognize it, triggering a recompression. One other constraint is that these bubble chambers have to have a strong background rejection.

The direct detection of a dark matter particle interaction is considered to be a rare event search since its expected rate is $\sim 3 \times 10^{-6}$ ev/Kg^{-1}day^{-1} meaning, 1 ev/ton^{-1}year^{-1}.

With statistics like this one, its crucial that background events are reduced to the smallest value possible, and this starts by shielding the detector, not only in its vicinity but also, performing the measurements underground.

The bubble chambers are threshold devices, and their critical energy and stopping power thresholds are tunable parameters, since they depend on the degree of superheat of the liquid. For liquids with high degrees of superheat, nearly any energy deposition induced by a radiation will nucleate a bubble, electron recoils included. But when the degree of superheat is modest, electron recoils no longer have enough stopping power to be above threshold, leaving only nuclear recoils (such as those produced via WIMP scattering) as capable of creating bubbles in the detector. This powerful built-in discrimination makes bubble chambers competitive dark matter detectors.

B. SIMPLE Experiment

The energy threshold curves of Fig.3 were calculated using eq.4, where dE/dx was estimated using monte carlo simulations. SIMPLE operates at 9°C, therefore, the threshold energy for nuclear recoils is 8 KeV when operating at 2 bar and 15 KeV when operating at 2.5 bar.

For this operating temperature, SIMPLE expects to see alpha particles with energies comprised roughly between 300keV and 1500 keV. Although, if the pressure is raised 0.5 bar, it expects to see no alphas at all.

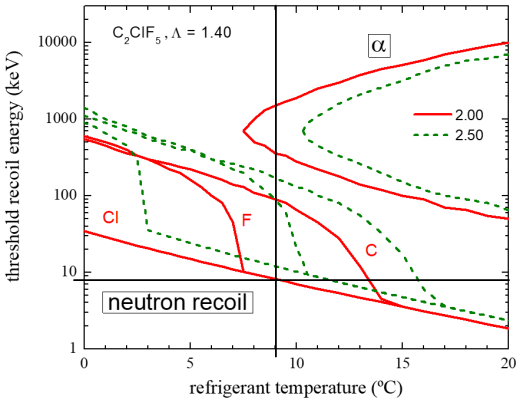

FIG. 3: Threshold energy curves for Cl, F and C for two different pressure values. The red line corresponds to 2 bar and the dashed green line, to 2.5 bar.

In Fig.4, the same analysis was made, only now considering different SHL based on halocarbons.

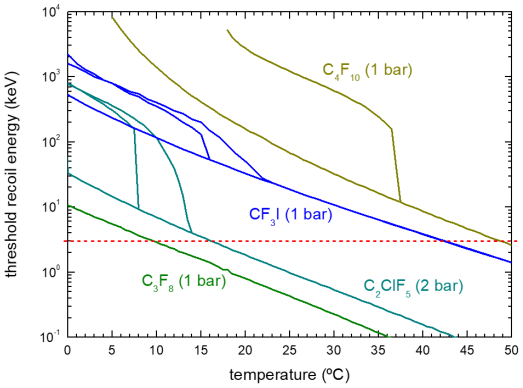

FIG. 4: Threshold energy curves for four different superheated liquids.

Considering the same 8 KeV for threshold energy, the value of the operating temperature changes according to the SHL used.

A unified parametrization of the properties of superheated liquid detectors, based on halocarbons has been proposed by d'Errico [7], where he introduces a non-dimensional quantity called "reduced superheat". This is defined as,

$$s = \frac{T - T_b}{T_c - T_b} \tag{5}$$

where T_b and T_c are boiling and critical temperatures of the liquid, respectively and T is the operating temperature. The introduction of this parameter causes the device response to occur all on a "universal" curve, independently of the liquid used.

Figure 5 shows the detector sensitivity to neutrons and photons as a function of the reduced superheat, for several SHL.

It is possible to observe that, operating at $s < 0.5$, the detector is insensitive to photons, as well as electrons, muons, gammas and other minimum-ionizing radiation not shown on the graph. And this happens independently

of the refrigerant basis (although this threshold occurs at different temperatures for different refrigerants).

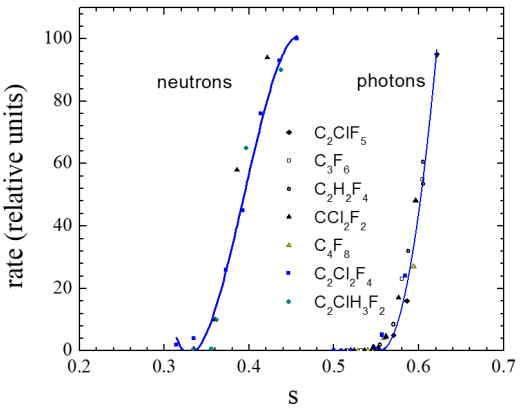

FIG. 5: Detector sensitivity as a function of reduced superheat for several SHL.

IV. BUBBLE CHAMBER DEPLOYMENT

A prototype of a bubble chamber (BC) has been developed by the SIMPLE Collaboration and the results were positive – it is possible, with the SIMPLE expertise and budget, to create a competitive BC for DM searches [8, 9]. My work is based on the knowledge learnt with the pioneer BC experiments made by the SIMPLE team and consists precisely on the deployment of a larger bubble chamber with improved operation conditions, to work as a dark matter detector.

The first step towards a BC detector construction is to choose an appropriate container. The material and geometry of the chamber must be such that it withstands the pressure recompression cycles necessary for its operation.

As a container for this DM detector, a $\sim 1,7$L PET (polyethylene terephthalate) recipient, resistant up to 16 bar of pressure, which is sold commercially for water filtration systems, was used. These types of containers are the ones usually used by the SIMPLE Collaboration, the only difference is that the previous ones could only go up to 10 bar of pressure and the one employed in this work goes up to 16 bar. This rise in maximum pressure is absolutely crucial when it comes to a BC detector with the amount of active mass used in this work. The recompression system needs to be powerful and fast enough to operate this detector without enormously increasing its dead time.

A. Detector's Body

- Purified food-based Gel

  Consists of an inexpensive mixture of three ingredients, carefully studied and combined by the SIMPLE Collaboration to create a visco-elastic substance capable of withstanding the nucleations in an SDD matrix [10]. In this BC project, the same gel is used, with the same purpose and two others. Namely, this is the substance used to sheath the walls of the containment vessel to prevent wall-induced heterogeneous nucleations from happening, and also maintain a distance between the container wall and the active mass.

- Halocarbon Superheated Liquid

  This constitutes the active mass of the detector. For this work, two superheated liquids were studied, C_2ClF_5 and C_3F_8.

- Purified Glycerin

  This is one of the ingredients of the purified gel recipe, it is used to enhance the viscosity and strength of the gel. In the context of a BC detector, it is also used as the buffer liquid, applying or removing pressure to the chamber.

The gel consists of a blend of 1.76% of powdered gelatin (Sigma Aldrich G-1890 Type A), 3.62% of PVP (Sigma Aldrich PVP-40T), 16.1% of bi-distilled water and 78.52% of glycerin (Riedel-de-Haën No.33224). Once made, the gel has a melting point of $\sim$35°C and becomes a gel around 30°C.

The process of gel fabrication consists of mixing, separately, glycerin and PVP with bi-distilled water allowing the mixture to blend, inside a *marie bath*, at a temperature of approximately 60°C, using a magnetic stirrer plate and a stirrer bar to agitate the mixture during all the process. After $\sim$ 20 minutes, when both solutions look homogeneous, one blends them together at a temperature of 70°C and leaves the misture inside a *marie bath* with a stirrer bar for 1h30. The viscous liquid obtained after this process, becomes a gel bellow 30°C.

Before sheathing the walls of the detector with this gel, one has to purify it in order to remove possible impurities (actinides) that would create unwanted nucleations. The purification process is the same for both the gel and the glycerin used. The purification technique uses resins that, once washed collect the actinides in the liquid. These are poured inside the desired liquid, the suspension is left with the agitation turned on for 12-15 hours. To take the resins out, one must filter the solution. To sheath the container, this was placed on a tripod with a big glass tube inside, without touching any part of it, with the help of a vertical stand and a clamp. Then the gel was poured inside in the interval between the glass tube and the chamber. Letting this apparatus dry to for 24-48 hours, for the gel to gelify properly, the glass tube was taken out . Once the walls were coated, purified glycerin was poured inside and the chamber's cap was screwed in, already with the appropriate connections made (Fig.6).

B. Detector's Cap

In order to operate the detector, this should be equipped with three lines of action: one for the freon filling/releasing, other for the glycerin entrance/exit and a last one to introduce a transducer to measure the pressure inside the chamber.

The connections used highly depend on the chamber chosen to do the work. In Fig.6 it is possible to see the cap of the detector built, which is constituted by a cylindrical

FIG. 6: Chamber on a tripod, with all the connections of the cap assembled.

metal part with two 3/4" cylindrical exits. Using several *swagelok* fittings, it was possible to decrease the diameter of the exit to fit in a 1/4" *festo* tube, creating the freon filling/releasing line. A teflon valve was attached to this line to allow the control of freon flow, this line ends with a quick connector, ready to be linked to the one on the freon bottle. On the opposite side of the freon line, lies the glycerin and transducer lines. In order to complete these lines, some *swagelok* fittings were used, along with a 1/2" *festo* tube. To create two different lines in only one access to the chamber, a T-connector was used, being able to link the transducer in one arm and create a glycerin line on the other.

With the detector closed, inside a 9°C bath, the rest of the chamber and the automaton system were filled with glycerin. The only part missing was to place the freon inside. To do so, the freon was first trespassed from the big bottle in the laboratory to a small portable one, and then, using this small one it was trespassed to the chamber. In total, $\sim$ 300 g of freon were put inside.

C. Automaton

The automaton that controls the bubble chamber detector is essentially operated with two glycerin pistons. Both of these *Festo* components compress or release pressure of the chamber as the software demands, and are compressed with pressurized N_2 gas. The automaton was built with two pressure lines, where each one takes advantage of only one piston, the blue line is used for low pressure values (Fig.7) and the green one for the higher pressure values (Fig.8). Connecting all the components, several high pressure *Festo* tubings, connectors, and fittings were used. Figs. 7 and 8 present a real picture of the automaton that controls the chamber operation and it's possible to see all these connectors and fittings in detail. To help compensate the glycerin flow, the system has incorporated a glycerin reservoir with the capability to purge unwanted N_2 from the system.

The interface with the automaton is made using a soft programming software built with Crouzet Logic Software

FIG. 7: Real picture of the automaton's blue line, where the piston goes from 2 to 8 bar. The N_2 gas used to compress the piston gets in the system through the tube on the right, straight up to EV1. This EV is the one controlling the amount of N_2 used to compress the blue piston and EV2 releases the N_2 when the chamber is decompressing. The tube on the upper left corner is the one going straight to the chamber to apply the pressure changes made by both pistons. EV3 applies the pressure changes made by the blue piston and EV6 applies the ones made by the green piston. **Caption:** 1- blue piston, 2- L-connector (elbow), 3- Y-connector, 4- glycerin reservoir, 5- T-connector, 6- manual valve, 7- purge, 8- blanking plug, 9- cap.

M3. The two necessary routines to operate the bubble chamber were created using this software. After many changes and different versions, the routine OPEN Valves allows the user to control the opening and closure of all the electrovalves of the automaton, and the routine Chamber Operation is the one used for the chamber's normal operation.

Routine: OPEN Valves

This routine allows the user to control which EV's are open and which are closed. When operating the bubble chamber, there are some actions that require a manual intervention, such as leveling the pistons or add/remove glycerin, and this must be done with some of the EV's open and others closed. Since the EV's used in the setup are, by default, closed, this routine is essential when making adjustments. Once this routine is active, the user can also open or close the EV's manually, using the buttons of the display.

Routine: Chamber Operation

The bubble chamber is operated in a cyclic way: start $\rightarrow$ compress $\rightarrow$ decompress $\rightarrow$ wait for events $\rightarrow$ start.

Both, the compression and decompression involve work from the blue and the green pistons, and each one needs some time to stabilize before changing piston. Through-

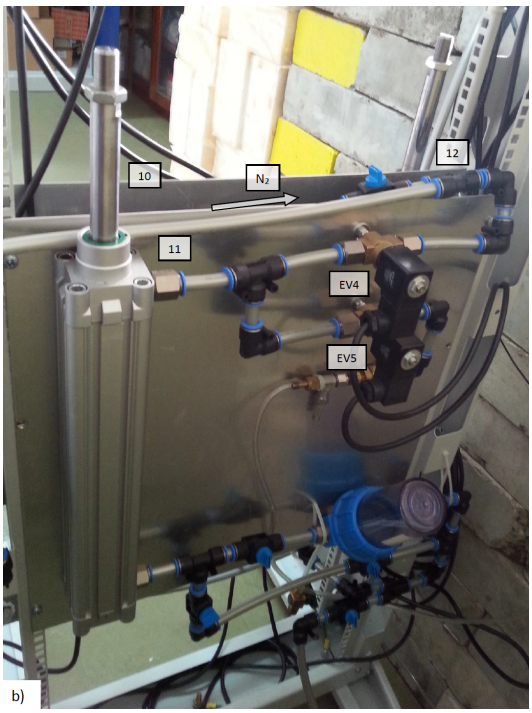

FIG. 8: Real picture of the automaton's green line, where the piston goes from 8 to 16 bar. This line stands on the back of the blue one so now the N_2 entrance stands on the left, becomes horizontal and goes directly to EV4. EV4 controls the entrance of N_2 to the green piston and EV5 releases it. **Caption:** 10- green piston, 11- fitting 12- push-in connector (link).

out all the operation, a safety block is actively comparing the pressure inside the chamber with a pressure break value. If it finds that the pressure of the chamber equals or transcends the break pressure, the program immediately forces a decompression.

This routine has four input parameters that the user must set before running it, the $\mathbf{P_{Max}}$ which corresponds to the pressure at which the system does the recompression (16 bar); $\mathbf{P_{Half}}$ corresponds to the value of pressure at which the automaton switches from one piston to the other (8 bar); **Op. P.** which is the operation pressure; and $\mathbf{P_{Diff}}$ which corresponds to the amount of pressure above the operation pressure considered for an event to have happened (300 mbar).

This routine communicates with the display block of the automaton showing the live pressure inside the chamber, and the number of recompressions each piston made, corresponding to the number of events that happened.

D. Recording Devices

The events are recorded via two channels: acoustically, using two different types of microphones and one hydrophone, and visually using a GoPro camera.

The shock wave produced by the bubble nucleation and expansion can be recorded by an acoustic sensor and then converted into an electrical pulse. This pulse tends to be a damped sinusoidal with a typical duration of several milliseconds. The COUPP experiment demonstrated [11], the sound of the acoustic event associated with a gas bubble nucleation in a bubble chamber shows a broad emission up to a frequency of 250kHz.

To record the bubble nucleation events, the following acoustic devices were used:

- An ultrassound, externally-polarized condenser microphone (CM16/CMPA40-5V from Avisoft-Bioacoustics) with a flat response over the 10 – 150 kHz frequency range, to record the shock wave associated with protobubble formation;
- A low frequency microphone, from Panasonic (omnidirectional) with flat frequency response over the range of 0.020 – 16kHz (3dB), with a signal-to-noise ratio (SNR) of 58 dB and a sensitivity of 7.9 mV/Pa at 1 kHz.
- An hydrophone (Reson) with a flat response over 5 – 170 kHz.

To visually record the events, a GoPro Hero 5 black edition camera, waterproof resistant up to 30 feet of depth, with a system of focus free and a maximum video resolution of 3840 x 2160 with 30 frames per second was used.

To make the bridge between the electronic devices and the computer acquiring the data, a digitizer NI-DAQ was used. In order to meet the range of the three microphones used, the DAQ board employed was the NI PCI-6251 16-Bit, with at least 1.25 MSps for 1-Channel.

E. Experimental Apparatus

The detector must be inside a water bath to allow the control of the temperature (Fig.9). All the water used for the bath is constantly being filtrated with a water filter to avoid the creation of silt and slime. The temperature is guaranteed and controlled by a cold finger, from Huber, and a polystat, from BioBlock, that also circulates the water around. To measure the exact temperature of the chamber, a laser thermometer FI 622TI, was used. Surrounding the chamber, there are several concrete blocks as well as paraffin ones to assure the safety of the user as well as the integrity of the laboratory in case on an accident and to provide some background shielding.

FIG. 9: Chamber inside the water bath. The polystat is visible as well as the cold finger and the water filter.

F. Prototype I

A first attempt to build a BC detector was made. The initial plan for this work was to use a big chamber, $\sim$ 30L of capacity, and construct the detector with it. Working with this chamber would for sure guarantee a gigantic increase in active mass, however it became impracticable to build a DM detector in such a chamber.

Following the procedure described earlier, the detector's body and cap were built and the experimental apparatus was settled. However, once an initial phase of tests started, to try to correlate the nucleations captured by the GoPro camera, the recompression made by the automaton and of course, a signal in the hydrophone channel, this correlation could not be obtained.

A lot of hypothesis were placed to try to explain this problem. Some of the conclusions drawn were the following:

- A chamber with $\sim$30L of capacity is too large and one could only see inside it through a small window, which makes the diagnosis of the problems difficult.
- All the pressure necessary to compress the freon, once an event occurred, was made through a small orifice. This caused the glycerin to enter the chamber with a certain speed, concentrated in a small region instead of creating a force applied to the entire surface of glycerin.
- The chamber could accumulate freon at the surface, because once it got there, it would hardly come down.
- Since it was a first trial out experiment, in the SIMPLE laboratory, to use such a big chamber, it was also the first time to use such a big bath. However, the cold finger available was not enough to achieve the cold temperature of 9°C at which one wanted to work.

Due to all these problems it became impracticable to use this chamber as a dark matter detector at this time. Valuable lessons were learned that immediately were put into practice and the building of a second prototype, to be used as the desired detector, started.

G. Prototype II

In order to build prototype II, the procedures described in the previous sections was followed. In Fig.10 it is possible to see the hydrophone attached to the chamber's wall. The low and high frequency microphones stood on top of the chamber, outside water, since these are not water resistant.

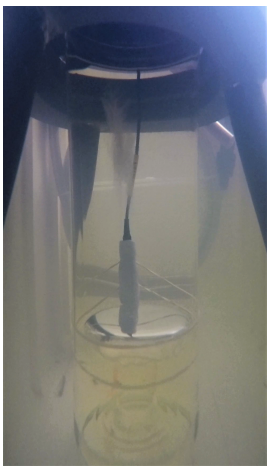

FIG. 10: Hydrophone attached to the chamber's wall, inside the water bath.

The result of the prototype II construction was a chamber with 1.7L of capacity, with $\sim$300g SHL freon as its active mass, which started to be C_2ClF_5 and then it was changed to C_3F_8 to obtain results with a different freon. The main differences from this chamber regarding the previous one, is that this one is much smaller, which allows a better control of the bath temperature. One other advantage is that this chamber is completely transparent which allows a visual inspection of the problems that get in the way of its good functioning.

This chamber was suitable to work as a dark matter detector and it performed according to the expected.

V. SIGNAL & RESULTS ANALYSIS

After studying the background noise of the laboratory, tests to the acoustic recording devices were performed, first by using the function generator and afterward by simulating nucleations creating air bubbles inside water with a straw. The result of these initial tests allowed me to take conclusions about the quality of the signal acquired by the three acoustic recording devices, and analyze possible time delays, shifts or malfunctionings.

The functioning of the three acoustic devices used was understood, a pressure stability test was performed to the chamber to guarantee that it was stable enough to only trigger events at the operation pressure. The test was successful and so one proceeded to the acquisition of nucleation signals. Figure 11 show a typical 10 minute acquisition. It is visible that every time the pistons are requested to do the work in the chamber, the acoustic devices record a noise. This noise is precisely associated with the input/release of N_2 gas into the system, used to operate the pistons.

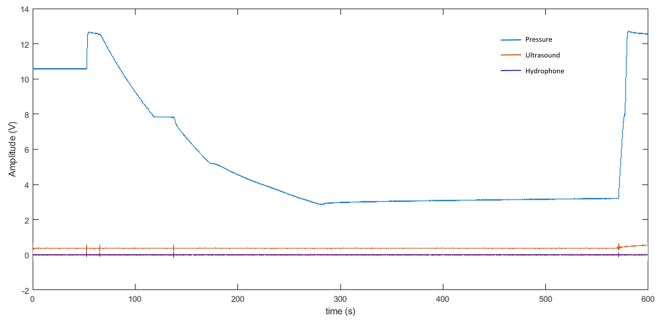

FIG. 11: Typical Acquisition.

In order to find the event, one has to look before the pressure rise (recompression) and before the piston noise associated with it. After manually finding a symmetric peak, one has to isolate it and recur to Matlab to find its beginning and end in time. With the peak isolated in time, one applies a Fast Fourier Transform (FFT) to determine its frequency. The next step is to build a frequency filter around this value and apply it to the whole signal, obtaining a clearer visualization of the peak. An example is shown in Fig.12.

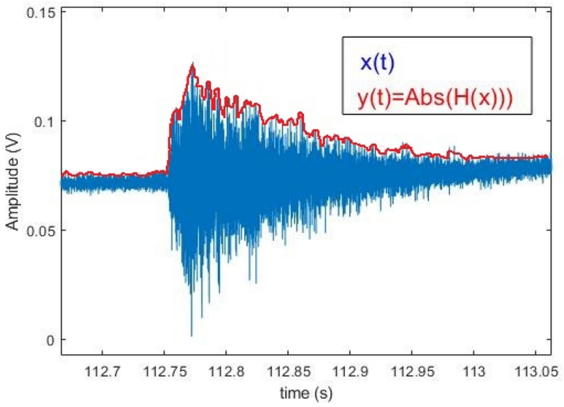

FIG. 12: Pulse signal of a typical event. In red it's represented the amplitude envelope.

To extract information about the characteristics of the event, one uses a simple pulse shape identification routine in which each pulse is first amplitude demodulated and then, its decay constant (τ) can be determined through an exponential fit.

The amplitude demodulation is reached by performing the modulus of the Hilbert transform of the pulse waveform, $y(t) = |H\{x(t)\}|$ giving the amplitude envelope. And τ can be obtained once found the maximum and minimum of the pulse shape, defining the time window of the pulse. The decaying part of the amplitude envelope is then fit to an exponential function, according to,

$$h(t) = Ae^{\tau \cdot t} \tag{6}$$

Figure 13 shows both the amplitude envelope and the exponential fit which allows to determine τ.

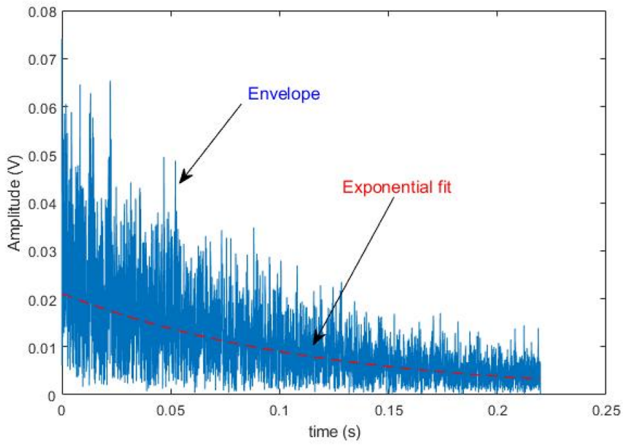

FIG. 13: Best fit of the exponential in Eq. 6 to the amplitude envelope of the pulse shown in Fig.12

After isolating a single nucleation event, as the one shown in Fig.12, and making a best fit of the amplitude envelope, the main Power Spectral Density (PSD) response is found at ∼4.4 kHz with a τ of ∼ 117.5 ms. This is the typical frequency spectrum of bubble nucleation signals.

A. Neutron & Alpha Calibrations

With the used conditions of pressure and temperature (2.5 bar at 9°C), the chamber is insensible to most atmospheric background radiation, remaining sensible to alpha particles and neutrons. The alpha particles will constitute the background events and the neutrons are thought to be particles with an experimental signature similar to the WIMPS, thus it is important to calibrate with these sources. With a study of the background radiation of the laboratory and the materials used, which has been done for the GESA facility in LSBB [12], one can predict the number of expected events and analyze if there was an excess, which could be related to a passage of a WIMP.

The SIMPLE Collaboration has done an extensive work in discriminating particle events with SDDs [13] and concluded that, it is possible to distinguish between an alpha particle and a neutron. They have different experimental signatures. Namely, the alpha produce more proto-bubbles, therefore create more energy inside a bubble nucleation, meaning the signal will have a larger signal amplitude than a neutron induced event. Such a discrimination work has been started using this bubble chamber, however, the calibrations performed lack in numbers to corroborate what was seen with the SDDs, since only a few tens of events were registered. For an accurate discrimination of event type signals, normally large hundreds of events are necessary, meaning a long period of acquisitions, which are not in the scope of this paper. In summary, this series of measurements using calibrated alpha and neutron irradiations should continue to confirm the ability to distinguish both event types acoustically.

The tests using the weak $AmBe$ (0.1 mCi) neutron source were performed carefully placing the source inside the laboratory and shielding it with polyethylene plates.

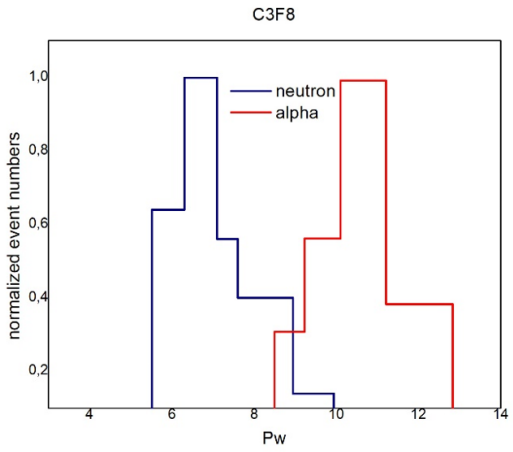

FIG. 14: Histogram presenting the calibrations made using alpha-particle and neutron sources.

It stood at a distance of approximately 50 centimeters from the chamber.

The overall frequencies and time constants found to be approximately $4-15$ kHz and $75-150$ ms, respectively. As for the amplitudes of the acoustic pulses, these vary between $15-140$ mV. These results are highly dependent on the size of the bubble that is formed upon radiation deposition. From what was observed visually, and recorded via the GoPro camera, smaller bubbles have lower amplitude signals and time constants, but higher frequencies. Larger bubbles give us the opposite result.

After doing the neutron calibrations, what followed was an alpha calibration with a liquid source, which was introduced via the Freon injection line at Freon injection conditions as described earlier.

The frequencies of the events oscillate between $\sim$5 and 17 kHz and have time constants that vary between $75-165$ ms. As for the amplitudes ($70-610$ mV), they are in the majority of the cases of higher amplitude ($> \sim 40\%$ – depending on the acoustic sensor) than the neutron induced ones, thus having added power. The variation behavior for the amplitudes, time constants and frequencies is the same as the one found, and mentioned before, for the neutron-induced events, suggesting a strong relation between these parameters and the size of the bubble that is formed.

For comparison purposes, in what follows, Fig.14 show an histogram considering the normalized number of events as a function of power. The power is directly related with the pulse amplitudes A, in mV, of the events and can be calculated according to,

$$P_w = ln(A^2) \tag{7}$$

These results were obtained at 2.75 – 3.00 bar and 12-16°C.

As one can see from Fig.14, there isn't yet a full discrimination between the events induced by alpha particles and the ones induced by neutrons. A possible reason for this to be happening, à priori, is the fact that the experiments were not performed under the same conditions of temperature.

VI. CONCLUSION

During the work with the SIMPLE Collaboration, the acquisition of a chamber that allows to be operated at higher pressures (16 bar) than the ones used previously in the SIMPLE laboratory (10 bar) was performed. This allows the chamber to be recompressed faster and more efficiently, reducing the detector dead time by a factor of 6 (compared to the previous 10 bar).

The existing automaton system was reconstructed and the creation of two routines to allow its operation was performed.

To instrument the bubble chamber, two new acquisition channels were introduced, assured by two different recording devices. The visual acquisition channel is assured by a water resistant camera that is able to accompany the detector underwater, into the bath, and record the events live. The acoustic channel, was enriched by the presence of an hydrophone that is also able to accompany the detector inside water, or even be placed inside it, to record the events directly from the inside. The acquired signal from the hydrophone was compared with the signals acquired from two extended microphones placed outside the chamber.

Hints of a possible discrimination between α-particles and neutrons have been shown, although additional investigations have to be performed, the path for this optimized detector is clearly the path for dark matter searches.

[1] Planck Collaboration. *Planck 2015 results. I. Overview of products and scientific results.* 2015.

[2] Felizardo, M. et al. *R&D of a SIMPLE bubble chamber for dark matter searches.* E3S W. C. 12, 3002, 3–8, 2016.

[3] SIMPLE Collaboration. *The SIMPLE Phase II dark matter search.* PHYSICAL REVIEW D 89, 072013 (2014). & *Final Analysis and Results of the Phase II SIMPLE Dark Matter Search.*Phys. Rev. Lett. 108, 201302 (2012).

[4] PICO Collaboration. *Dark Matter Search Results from the PICO-60 C_3F_8 Bubble Chamber.* 1–6, 2017.

[5] F. Seitz *On the Theory of the bubble chamber.* Physics of Fluids 1, 2-13. 1958.

[6] D. A. Fustin *First Dark Matter Limits from the COUPP 4 kg Bubble Chamber at a deep underground site.* 2012.

[7] F. d'Errico. *Fundamental Properties of Superheated Drop (Bubble) Detectors.* Radiation Protection Dosimetry, Vol. 84, Nos. 1–4, pp. 55–62 (1999).

[8] A.R. Ramos et. al. *A SIMPLE Bubble Chamber for Dark Matter Searches: Testing and Development.* 2015 4th International ANIMA Conference.

[9] M. Felizardo et. al. *R&D of a SIMPLE bubble chamber for dark matter searches.* E3S W.C. 12, 03002, i-DUST 2016.

[10] M. Felizardo et. al. *Superheated droplet detector response to fabrication variations.* Nucl. Instr. and Meth. Physics Research A 614, 278–286, (2010).

[11] COUPP Collaboration *First dark matter search results from a 4-kg C_3FI bubble chamber operated in a deep underground site.* Phys. Rev. D, vol. 86, no. 5, pp. 052001, (2012).

[12] A. C. Fernandes et. al. *Neutron background signal in superheated droplet detectors of the Phase II SIMPLE dark matter search.* Astroparticle Physics, Vol 76, March 2016, P. 48-60.

[13] Felizardo, M. *Neutron – Alpha irradiation response of superheated emulsion detectors.* Nucl. Instr. and Meth. Physics Research A 863 (2017) 62–73.